National Research Council Canada
Conseil national de recherches Canada

SUBSONIC WALL INTERFERENCE CORRECTIONS FOR HALF-MODEL TESTS USING SPARSE WALL PRESSURE DATA

by
M. Mokry
National Aeronautical Establishment

OTTAWA
NOVEMBER 1985

Canada

AERONAUTICAL REPORT
LR-616
NRC NO. 25132

NATIONAL AERONAUTICAL ESTABLISHMENT

SCIENTIFIC AND TECHNICAL PUBLICATIONS

AERONAUTICAL REPORTS:

Aeronautical Reports (LR): Scientific and technical information pertaining to aeronautics considered important, complete, and a lasting contribution to existing knowledge.

Mechanical Engineering Reports (MS): Scientific and technical information pertaining to investigations outside aeronautics considered important, complete, and a lasting contribution to existing knowledge.

AERONAUTICAL NOTES (AN): Information less broad in scope but nevertheless of importance as a contribution to existing knowledge.

LABORATORY TECHNICAL REPORTS (LTR): Information receiving limited distribution because of preliminary data, security classification, proprietary, or other reasons.

Details on the availability of these publications may be obtained from:

Publications Section,
National Research Council Canada,
National Aeronautical Establishment,
Bldg. M-16, Room 204,
Montreal Road,
Ottawa, Ontario
K1A 0R6

ÉTABLISSEMENT AÉRONAUTIQUE NATIONAL

PUBLICATIONS SCIENTIFIQUES ET TECHNIQUES

RAPPORTS D'AÉRONAUTIQUE

Rapports d'aéronautique (LR): Informations scientifiques et techniques touchant l'aéronautique jugées importantes, complètes et durables en termes de contribution aux connaissances actuelles.

Rapports de génie mécanique (MS): Informations scientifiques et techniques sur la recherche externe à l'aéronautique jugées importantes, complètes et durables en termes de contribution aux connaissances actuelles.

CAHIERS D'AÉRONAUTIQUE (AN): Informations de moindre portée mais importantes en termes d'accroissement des connaissances.

RAPPORTS TECHNIQUES DE LABORATOIRE (LTR): Informations peu disséminées pour des raisons d'usage secret, de droit de propriété ou autres ou parce qu'elles constituent des données préliminaires.

Les publications ci-dessus peuvent être obtenues à l'adresse suivante:

Section des publications
Conseil national de recherches Canada
Établissement aéronautique national
Im. M-16, pièce 204
Chemin de Montréal
Ottawa (Ontario)
K1A 0R6

SUBSONIC WALL INTERFERENCE CORRECTIONS FOR HALF-MODEL TESTS USING SPARSE WALL PRESSURE DATA

CORRECTIONS SUBSONIQUES DES EFFETS DE PAROIS POUR DES ESSAIS DE DEMI-MAQUETTES À L'AIDE DE DONNÉES DISPERSÉES DE PRESSION SUR LES PAROIS

by/par

M. Mokry

Presented at the Euromech Colloquium No. 187 *Adaptive Wall Wind Tunnels and Wall Interference Correction Methods*, Göttingen, October 15-17, 1984.

Présenté au colloque Euromech n° 187 *Adaptive Wall Wind Tunnels and Wall Interference Correction Methods*, Göttingen, 15-17 octobre 1984.

L.H. Ohman, Head/Chef
High Speed Aerodynamics Laboratory/
Laboratoire d'aérodynamique à hautes vitesses

G.M. Lindberg
Director/Directeur

SUMMARY

A method is described for correcting subsonic wind tunnel measurements on half-models in ventilated test sections, operated at subcritical flow conditions at the walls. For perforated walls, the boundary values of the streamwise component of the wall interference velocity are obtained from static pressures measured by a few longitudinal pressure tubes or rails attached to the walls and from the estimated farfield of the model in free air. The sparse boundary data is extended by means of streamwise smoothing and transverse interpolation. The streamwise velocity correction is derived from the doublet panel solution of an interior Dirichlet problem and the transverse corrections by integrating the irrotational flow conditions.

The evaluated corrections to Mach number and angle of attack, presented as contour plots in the wing plane, provide insight into the correctability of the test results. Examples are given for a transport aircraft half-model tested in the NAE high speed wind tunnel. Applicability of the method at supercritical flow conditions at the model is examined on experimental and computational data of a high aspect ratio wing in the Lockheed CFWT facility.

RÉSUMÉ

On décrit une méthode de correction de mesures subsoniques effectuées en soufflerie sur des demi-maquettes placées dans des veines d'essai ventilées, dans des conditions d'écoulement subcritique sur les parois. Pour des parois perforées, les valeurs limites de la composante longitudinale de la vitesse de perturbation induite par les parois sont obtenues à partir des pressions statiques mesurées par quelques tubes de pression longitudinaux ou par des rails fixés aux parois et à partir du champ lointain estimé du modèle à l'air libre. Les données limites dispersées sont augmentées au moyen d'un lissage longitudinal et d'interpolations transversales. La vitesse longitudinale est corrigée par résolution d'un problème intérieur de Dirichlet par la méthode des doublets et la vitesse transversale par intégration des conditions d'écoulement irrotationnel.

Les corrections évaluées du nombre de Mach et de l'angle d'incidence, présentées sous forme de contours dans le plan de l'aile, renseignent sur la mesure dans laquelle on peut corriger les résultats des essais. Des exemples sont donnés pour une demi-maquette d'avion de transport essayée dans la soufflerie à vitesse élevée de l'EAN. L'applicabilité de la méthode à des conditions d'écoulement supercritiques sur la maquette est examinée à partir de données expérmentales et calculées pour une aile à allongement élevé placée dans la soufflerie à écoulement compressible (CFWT) de Lockheed.

CONTENTS

TABLES

ILLUSTRATIONS

ILLUSTRATIONS (Cont'd)

APPENDICES

SYMBOLS

A	model reference area or system matrix
A, B	half-axes of the Rankine body
C_D	model drag coefficient
C_L	model lift coefficient
C_p	pressure coefficient
E	eccentricity of the Rankine body
f	doublet density
M	stream Mach number
$\overline{n}$	outward (unit) normal vector
$\overline{r}$	position vector
S	test section boundary
u, v, w	components of wall interference velocity
V	test section volume or wing volume
X, Y, Z	Cartesian coordinates in the physical plane
x, y, z	Cartesian coordinates in the transformed plane
α	angle of attack (deg)
β	Prandtl-Glauert factor
γ	ratio of specific heats
Γ	wing circulation
δ	Dirac delta function
Δ	wall interference correction
μ	source (sink) strength of the Rankine body
ξ, η, ς	local coordinates
σ	wing source strength
ϕ	disturbance velocity potential
ψ	sideslip angle (deg)

Subscripts

F	free air part
j, k	collocation points
m	wing element point
o	observation (field) point
R	reference plane
W	wall interference part
$1, 2$	panel corners

Superscripts

B	associated with Rankine body
D	associated with drag
L	associated with lift
V	associated with volume

1.0 INTRODUCTION

The introduction of wind tunnels with adaptive walls, making extensive use of measurements of flow parameters on control surfaces, gave a new impetus for the development of more rigorous correction methods for conventional wind tunnels. After several decades of testing and comparisons of theory with experimental results it became evident that application of idealized boundary conditions representing flow through ventilated walls was inadequate. Capelier, Chevallier, and Bouniol gave a pioneering paper [1] on the subject, showing that with the help of measured wall pressures and the farfield representation of the model by singularities, it is possible to obtain subsonic corrections as a solution of the interior Dirichlet problem, with no reference to the crossflow properties of the walls.

For solid walls, a method utilizing wall pressure measurements was independently proposed by Ashill and Weeks [2]. The major difference between the two techniques is due to the fact that at a solid wall the velocity vector is fully determined by static pressure. The corrections can be obtained from Green's theorem, making the farfield representation of the model superfluous. Hackett et al.[3] showed that for solid walls the location of model singularities and their strengths can in fact be deduced from wall pressure signatures alone. The advantage of not requiring the simulation of the model farfield is of particular benefit in cases where the flows are complex and hence are not easily modeled, for example those with extensive separations. The method of Ref.[2] is in principle also applicable to ventilated tunnel walls, however, a fast, reliable measurement the boundary flow angles is still an unresolved problem.

The "inordinate" amount of experimental data, needed to specify (Dirichlet) boundary values on bounding surfaces, appears as an obstacle to the three-dimensional interference assessment [4]. Fortunately, physics of pressure disturbance propagation and direct wind tunnel observations indicate that wall interference effects are in general less severe in three dimensions than those in two dimensions. Accordingly, simplifying assumptions can be made to develop cost-effective procedures that minimize the number of boundary measurements needed to assess wall interference [5]. Thus Ref.[1] suggests to use the Fourier expansion of the sparse pressure data on the bounding surfaces, showing that that in fact only a first few terms are required to achieve an acceptable accuracy. Sawada [6] devised a similar technique, giving a comprehensive analysis of the weight functions of the Fourier components. Mokry [7] represented the model by a point disturbance and evaluated the corrections from the Fourier solution for the Dirichlet problem in a finite-length circular cylinder. Wall pressures measured by four longitudinal pressure tubes were used to define the lowest order harmonics, that proved to be sufficient for defining the Mach number and the flow angle corrections at the model position. Conceivably, this technique is limited to small models in test sections permitting the placement of pressure tubes on a cylindrical surface, such as those having circular, octagonal or square cross-sections. The method of Rizk and Smithmeyer [8], developed during the same period, is applicable to general rectangular cross-sections and uses a more realistic representation of the test model. Static pressures are assumed to be known all over the test section boundary, using a combination of sparse measurements and theoretical estimates. A potential flow model of a slotted wall test section, intended for use with sparsely measured wall pressues, has more recently been

proposed by Kemp [4]. While this approach is suitable for longitudinally slotted walls, preserving streamwise momentum, it is apparently not applicable to perforated walls, having viscous cross-flow properties.

The present method is devised for rectangular tunnel cross-sections and has many common features with that of Ref.[8]. For perforated test section walls, the boundary pressures are assumed to be measured by a number of pressure tubes or rails, Fig.1, attached directly to the walls as shown on schematic diagrams in Fig.2. The rails, Fig.1b, by the nature of their design [9], are excellent static pressure devices for two-dimensional testing, but the simpler tubes, Fig.1a, appear to be more tolerant to three-dimensional disturbance fields, such as generated by half-models. An asymptotic analysis [10] of tube surface pressures indicates that the departure from the ambient static pressure (measurement error), being proportional to the product of the tube radius and the streamwise derivative of normal velocity, was in our case insignificant and could be ignored. From the point of view of applicability of the method, the most important feature was a relatively low scatter of the measured pressures, see a typical example in Fig.5, allowing to interpret them as "averaged" pressures over the open and closed portions of the walls. For longitudinally slotted tunnel walls, the use of similar pressure devices is very unlikely, as the pressure taps can directly be installed on the slats. The interpretation of slat pressures in terms of "averaged" boundary pressures is not as simple [4],[11],[12], but the implementation of the method is in principle as for perforated walls.

The boundary values of the streamwise component of wall interference velocity, obtained by subtracting the estimated pressure disturbance of the model in free air, are smoothed and expanded over the bounding surfaces in transverse directions by means of interpolations. The interior Dirichlet problem for the streamwise component of wall interference velocity is solved by the first-order doublet panel method. The transverse components of wall interference velocity are derived by integrating the irrotionality conditions and assuming that flow is parallel to the tunnel axis at a reference plane far upstream.

2.0 DESCRIPTION OF THE METHOD

It is stipulated that there exists a region between the tunnel walls and the model where the flow can be adequately described by the linearized potential equation *

$$\beta^2 \frac{\partial^2 \phi}{\partial X^2} + \frac{\partial^2 \phi}{\partial Y^2} + \frac{\partial^2 \phi}{\partial Z^2} = 0. \tag{2.1}$$

In accordance with the classical concept of subsonic wall interference [13], the disturbance velocity potential in the linearized flow region is decomposed into two terms:

$$\phi = \phi_F + \phi_W, \tag{2.2}$$

* One of the advantages of this method is that it only requires the linearized equation to be valid near the wall (excluding the shear layers). This means that the procedure may be valid as long as supersonic pockets do not extend to the tunnel walls.

where ϕ_F is the disturbance potential of the model in free air and ϕ_W is the disturbance potential, representing the effect of tunnel walls. It is further assumed that ϕ_W satisfies Eq.(2.1) in the entire tunnel interior, including the volume occupied by the model. The derivatives

$$u = \frac{\partial \phi_W}{\partial X}, \quad v = \frac{\partial \phi_W}{\partial Y}, \quad w = \frac{\partial \phi_W}{\partial Z} \tag{2.3}$$

are the *interference velocity components*, interpreted as disturbances to unit stream velocity. Of particular interest are their values at the model, which determine the local flow conditions to which the tested model is subjected. Because of differentiability of harmonic functions, the interference velocity components inside the test section again satisfy

$$\beta^2 \frac{\partial^2 u}{\partial X^2} + \frac{\partial^2 u}{\partial Y^2} + \frac{\partial^2 u}{\partial Z^2} = 0, \tag{2.4}$$

and so on.

If the static pressure is measured on the tunnel boundary, the boundary values of the streamwise component of wall interference velocity, u, can be obtained via the linearized pressure coefficient

$$C_p = -2 \frac{\partial \phi}{\partial X}. \tag{2.5}$$

From Eqs.(2.2) and (2.3)

$$u = -\frac{1}{2} C_p - \frac{\partial \phi_F}{\partial X}. \tag{2.6}$$

The streamwise derivative of ϕ_F on the tunnel boundary can be estimated from measured forces and model geometry as discussed in Appendix 1.

Provided that the values of u are known over a closed test section boundary, Eqs.(2.4) and (2.6) specify an interior Dirichlet problem, whose solution is known to exist and be unique.

The transverse velocity components, v and w, can similarly be determined from their respective (Dirichlet) boundary values. If, however, only the boundary values of u are known, the determination of v and w via irrotational flow conditions is nonunique. One sees immediately that if $\varphi = \varphi(Y, Z)$ is an arbitrary function satisfying Laplace's equation

$$\frac{\partial^2 \varphi}{\partial Y^2} + \frac{\partial^2 \varphi}{\partial Z^2} = 0$$

in the transverse Y, Z plane, then the sum $\phi + \varphi$ again satisfies Eqs.(2.1) and (2.5).

In two dimensions (absence of coordinate Y), the integration yields $\partial \varphi / \partial Z =$ constant and hence the transverse component of velocity, w, is determined from u only up to a constant [14]. In three dimensions, the interference velocity components v and w are determined from u to within an arbitrary solution of Laplace's equation in the transverse plane. Integrating the differentials dv and dw in the streamwise direction, we obtain [8]:

$$\begin{aligned} v(X, Y, Z) - v(X_R, Y, Z) &= \int_{X_R}^{X} \frac{\partial u}{\partial Y}(\xi, Y, Z) d\xi, \\ w(X, Y, Z) - w(X_R, Y, Z) &= \int_{X_R}^{X} \frac{\partial u}{\partial Z}(\xi, Y, Z) d\xi, \end{aligned} \tag{2.7}$$

where X_R is the X-coordinate of the (upstream) reference plane. Accordingly, v and w can be determined from Eqs.(2.7) at any point X, Y, Z inside the test section, provided that their reference-plane values are known. Flow angle measurement is a possibility [15], but it is unlikely that it could be done in "production" testing.

One of the simple options of bypassing the measurement is to assume that at a (distant) reference plane the flow is parallel to tunnel axis:

$$\begin{aligned} \frac{\partial \phi}{\partial Y}(X_R, Y, Z) &= 0, \\ \frac{\partial \phi}{\partial Z}(X_R, Y, Z) &= 0. \end{aligned} \tag{2.8}$$

In principle, the "zero flow angle conditions" (2.8) are justifiable for a distant reference plane in a closed wall test section, where the theoretical flow angle is known to decrease with the distance from the model by an order of magnitude faster than in free air. To examine their validity for a ventilated wall test section, we differentiate Eqs.(2.8) with respect to Y and Z and substitute them in Eq.(2.1). This shows that

$$\frac{\partial^2 \phi}{\partial X^2}(X_R, Y, Z) = 0,$$

or, in terms of the linearized pressure coefficient (2.5),

$$\frac{\partial C_p}{\partial X}(X_R, Y, Z) = 0. \tag{2.9}$$

Accordingly, Eqs. (2.8) are admissible as upstream boundary conditions if the measured streamwise pressure curves display zero slopes at the reference plane.

Inserting Eqs.(2.2) and (2.8) in (2.3), we obtain the reference-plane values

$$\begin{aligned} v(X_R, Y, Z) &= -\frac{\partial \phi_F}{\partial Y}(X_R, Y, Z), \\ w(X_R, Y, Z) &= -\frac{\partial \phi_F}{\partial Z}(X_R, Y, Z), \end{aligned} \tag{2.10}$$

that may be evaluated from the farfield of ϕ_F, see Appendix 1, and substituted in Eqs.(2.7).

Once the interior values of components of wall interference velocity have been computed, the wall interference corrections can be evaluated by standard procedures [16]. Thus the Mach number correction is obtained as

$$\Delta M = (1 + \frac{\gamma - 1}{2} M^2) M u, \tag{2.11}$$

where M is the reference Mach number (on which the pressure coefficients are based) and $\gamma (= 1.4)$ is the ratio of specific heats. The sideslip and angle of attack corrections (in radians) are directly the values of v and w respectively:

$$\begin{aligned} \Delta \psi &= v, \\ \Delta \alpha &= w. \end{aligned} \tag{2.12}$$

Usually, these corrections are evaluated at a representative model station (centre of loading), or as averages over the model. Additionally, flow nonuniformities that may be of relevance for large model dimensions can be expressed as spatial variations of Mach number and flow angle corrections [17].

3.0 DOUBLET PANEL METHOD

The classical method for solving the interior Dirichlet problem is to construct the solution in terms of a double layer distribution on the bounding surface. To facilitate this approach, we use the compressibility transformation

$$x = X, \quad y = \beta Y, \quad z = \beta Z \tag{3.1}$$

to reduce Eq.(2.4) to Laplace's equation, $\nabla^2 u = 0$. Introducing the position vectors

$$\bar{r}_o = (x_o, y_o, z_o) \qquad \text{and} \qquad \bar{r} = (x, y, z)$$

of the observation point and the running point respectively, the streamwise component of the wall interference velocity can be expressed in terms of a *double layer distribution*

$$u(\bar{r}_o) = \iint_S f(\bar{r}) \frac{\partial}{\partial n} \left(\frac{1}{4\pi |\bar{r}_o - \bar{r}|} \right) dS, \tag{3.2}$$

where S is the test section boundary, the scalar function f of the vector argument $\bar{r}$ is the *doublet density*, and $\partial/\partial n$ denotes the outward normal derivative. All differential and integral operations are performed with respect to the unsubscripted coordinates.

In the limit $\bar{r}_o \to \bar{r}_k \in S$, as the observation point $\bar{r}_o$ approaches a smooth surface point $\bar{r}_k$, Eq.(3.2) becomes the Fredholm integral equation of the second kind for the doublet density [18]:

$$u(\bar{r}_k) = -\frac{1}{2} f(\bar{r}_k) + \iint\!\!\!\!\!\!- _S f(\bar{r}) \frac{\partial}{\partial n} \left(\frac{1}{4\pi |\bar{r}_k - \bar{r}|} \right) dS. \tag{3.3}$$

The crossed integral sign is used to point out that a small area surrounding the point $\bar{r}_k$ is excluded from the surface integral. The integral equation is solved numerically, by approximating the surface by planar panels S_j, $(j = 1, \ldots, N)$, and using piecewise constant doublet densities,

$$f(\bar{r}) = f_j, \qquad \bar{r} \in S_j.$$

Since

$$\frac{\partial}{\partial n} \frac{1}{|\bar{r}_k - \bar{r}|} = \frac{\bar{n} \cdot (\bar{r}_k - \bar{r})}{|\bar{r}_k - \bar{r}|^3}$$

is zero if $\bar{r}_k \in S_k$, Eq.(3.3) reduces to

$$u(\bar{r}_k) = -\frac{1}{2} f_k + \sum_{\substack{j=1 \\ j \neq k}}^{N} f_j \iint_{S_j} \frac{\partial}{\partial n} \left(\frac{1}{4\pi |\bar{r}_k - \bar{r}|} \right) dS. \tag{3.4}$$

Selecting as collocation points $\bar{r}_k$ all panel centroids, we obtain a system of linear algebraic equations

$$\sum_{j=1}^{N} A_{kj} f_j = u_k, \qquad k = 1, \ldots, N \tag{3.5}$$

for the N unknown values of doublet densities f_j. The matrix element

$$A_{kj} = \begin{cases} -\frac{1}{2}, & \text{if } j = k; \\ \iint_{S_j} \frac{\partial}{\partial n} \left(\frac{1}{4\pi |\bar{r}_k - \bar{r}|} \right) dS, & \text{if } j \neq k \end{cases} \tag{3.6}$$

is evaluated for a rectangular wall panel in closed form in Appendix 2.

Once the doublet densities are known, the value of the streamwise component of the wall interference velocity at an arbitrary interior point $\bar{r}_o$ is calculated from

$$u(\bar{r}_o) = \sum_{j=1}^{N} f_j \iint_{S_j} \frac{\partial}{\partial n} \left(\frac{1}{4\pi |\bar{r}_o - \bar{r}|} \right) dS, \tag{3.7}$$

which is the discrete form of integral (3.2). The transverse components of wind tunnel interference velocity, v and w, are obtained using Eqs.(2.7) and (2.10).

An interesting property of the double layer distribution (3.2) emerges when setting $f(\bar{r}) \equiv -1$ on the bounding surface S. Converting the surface integral to a volume integral and using the fact that $-1/(4\pi|\bar{r}_o - \bar{r}|)$ is the fundamental solution for the Laplace operator, we obtain

$$\begin{aligned} u(\bar{r}_o) &= \iint_S \frac{\partial}{\partial n} \left(\frac{-1}{4\pi |\bar{r}_o - \bar{r}|} \right) dS \\ &= \iiint_V \nabla^2 \left(\frac{-1}{4\pi |\bar{r}_o - \bar{r}|} \right) dV \\ &= \iiint_V \delta(\bar{r}_o - \bar{r}) dV \quad = 1, \quad \bar{r}_o \in V, \end{aligned}$$

where V is the volume enclosed by the surface S and δ is the Dirac delta function. Conversely, if u is specified to be unity on the smooth portions of bounding surface S, then the corresponding doublet density f is minus one. This property can be used as a simple numerical check for the doublet panel program.

4.0 COMPLETION OF BOUNDARY DATA

Apart from the uncertainty of corrections utilizing the classical interference concept, the major source of inaccuracy of the method is due to the fact that the boundary values at panel centroids have to be constructed from the sparse data provided by a few pressure tubes attached to the walls. Based on some preliminary tunnel flow calculations [19],[20],

it was observed that evaluating the boundary values u from Eq.(2.6) along the pressure tubes, smoothing them, and interpolating in transverse directions gives a good chance of obtaining a meaningful approximation to the entire boundary data.

Four tubes located as shown in Fig.2a, allowing to capture spanwise variations of pressures in the top and bottom planes, were used by Digney [20] and Khalid [21] in NAE half-model tests. Using symmetry about the reflection plane, $\partial u/\partial y = 0$ at $y = 0$, two tubes per wall (T1, T3 and T2, T4) permit quadratic interpolation in the spanwise direction. If the sidewall is solid, it acts as an additional reflection plane, and cubic interpolation can be used. In the four-tube configuration of Fig.2a, the sidewall boundary values can be approximated by interpolating the extrapolated corner values at the top and bottom walls. If appreciable blockage effects are expected (bulky fuselage), additional sidewall tubes may be required, Figs.2b and 2c. The six-tube configuration in Fig.2c is proposed for the next phase of half-model measurements in the NAE 5 ft $\times$ 5 ft test section. An alternative six-rail configuration in Fig.2d, dictated by the elongation of the 20 in $\times$ 28 in cross section of the Lockheed-Georgia Compressible Flow Wind Tunnel (CFWT), was utilized by Pounds and Walker [22].

The completion of Dirichlet boundary values at the upstream and downstream ends of the test section may yet present another problem, since supplementary pressure measurements are difficult to make across the stream. Of course, if identical C_p values are attained at the endplanes by all tubes, C_p may be assumed constant at these planes and the boundary values of u evaluated quite simply from Eq.(2.6). Otherwise, interpolations of the earlier constructed edge values need to be employed.

5.0 APPLICATION OF THE METHOD

Following a successful verification of the method on the simple test procedure decribed at the end of Sect.3.0, the method was applied to actual half-model measurements in the NAE High Speed Wind Tunnel. The walls of the 5 ft $\times$ 5 ft transonic test section are perforated by normal holes of 0.5 in diameter, providing an open area ratio of 20%. Boundary pressures were measured by four 1 in diameter pressure tubes, Fig.1a, each containing 40 static pressure orifices. The tubes were mounted to upper and lower walls, as shown schematically on Fig 2a, with the pressure orifices facing the model (x, y plane). The transverse coordinates of the pressure orifices, displaced by the tube diameter from the walls, are given in Table 1. The streamwise distribution of pressure orifices will become apparent in the figures presenting wall panelling and measured pressure distributions.

The divisions of the test section boundaries into 72 and 200 rectangular panels, explored in the present paper, are shown in Figs.3 and 4. This "open box" panelling excludes the reflection plane, to which the model is mounted. The locations of pressure taps of the pressure tubes T1-T4 are indicated by rows of crosses on upper and lower boundaries. The measured static pressures along the tubes are plotted in Fig.5, for a typical example: $M = 0.60$ and $\alpha = 1.951^0$, corresponding to a measured $C_L = 0.689$. The corrections ΔM and $\Delta\alpha$ evaluated in the zero-incidence wing plane are shown in Fig.6 (72 panels) and Fig.7 (200 panels). The difference between the contour plots of Figs.5 and 6 is not large, so that

either of them can be used for a qualitative description. The Mach number correction is observed to be small and fairly uniform over the wing, which is important from the point of view of reliability of test data on this most sensitive component of the model. However, the variation of ΔM over the fuselage indicates the presence of a buoyancy force. Since the flow was accelerated over the model (a negative ΔM correction is required at the nose and a positive correction at the tail), the measured drag force was obviously larger than the one that would act on the model in free air. The angle of attack correction varies less than 0.1^0 over the wing span, which is within the limits of acceptance. Downstream gradients of ΔM and $\Delta\alpha$, corresponding to the drift of measured pressures towards negative values at the test section exit, see Fig.5, influence the model data only indirectly, via trailing shear layers. On the whole, the wind tunnel data appears to be "correctable" to free air data.

Table 1. NAE pressure tubes

Tube	y(in)	z(in)
T1	11.25	29.00
T2	11.25	-29.00
T3	44.25	29.00
T4	44.25	-29.00

A summary plot of ΔM and $\Delta\alpha$ versus the measured C_L, containing five different incidence cases, is shown in Fig.8. The symbols indicate correction values evaluated at the centre of theoretical wing loading. The relatively small differences between the 200 panel solutions (dark symbols) and the 72 panel solutions (open symbols) suggest that the coarser panelling can be used for a quick assessment of corrections by an on-line computer during wind tunnel tests.

Applicability of the method at supercritical conditions at the model was examined on the experimental and computational data [23] and [24] of a high aspect ratio wing "A", tested in the Lockheed-Georgia Compressible Flow Wind Tunnel (CFWT). The experimental data used here were released to AGARD as test cases for computers program assessment [25]. The walls of the CFWT 20 in $\times$ 28 in test section, perforated with 0.25 in diameter holes slanted 60^0 from the normal, were adjusted by moving outside shutter plates to provide a 4% open area ratio. Six pressure rails, each containing 31 pressure orifices and designed in smaller scale similar to Fig.1b, were used to measure static pressures at the test section walls. The rails were mounted above and below the model as shown schematically in Fig.2d. The actual y and z coordinates of the pressure orifices are given in Table 2. The experimental rail pressure distributions, obtained at $M = 0.82$ and $C_L = 0.53$, are presented in Fig.9. Together with the "A" Wing geometry [25], they provide sufficient input data for the evaluation of the corrections by the present method.

The Mach number correction of Hinson and Burdges [23],[24], obtained by an extended Bailey-Ballhaus transonic flow code [26], is used here for comparison. The method is based on matching the theoretical wing pressures computed using experimental pressure boundary conditions and free air (unbounded) conditions. The adjustments of free

stream Mach number and of angle of attack, required to establish agreement with the pressure-boundary-condition computation, define the corrections. For Wing "A", a simple correction to freestream Mach number of approximately $\Delta M = -0.005$ was found to provide an acceptable match [23],[24].

Table 2. CFWT pressure rails

Tube	y(in)	z(in)
T1	6.00	9.25
T2	5.56	-9.25
T3	12.93	9.25
T4	12.88	-9.25
T5	19.68	9.25
T6	19.62	-9.25

The corrections produced by the present panel method in Fig.10 indicate that the strip $-0.004 > \Delta M > -0.006$ extends over the central portion of the wing, and affirms that the measurement is correctable for blockage by an adjustment of -0.005 in Mach number. The angle of attack correction is observed to be less uniform, however, no comparison is available in Refs.[23] or [24] to confirm our result $\Delta\alpha \simeq -0.3^0$ near the centre of wing load.

6.0 CONCLUSIONS

A linear method has been developed for the evaluation wall interference corrections for half-model configurations at subcritical conditions at the ventilated test section walls. Input data required for the method are static pressures measured along several longitudinal rows of pressure orifices near or on the walls, global geometrical parameters of the model, and measured forces. Similarly to other methods based on model representation and measured pressure boundary conditions, the crossflow properties of the walls do not enter the problem explicitly. The technique is simple, straightforward, and suitable for a routine post-test assessment of corrections in test section with perforated walls.

7.0 ACKNOWLEDGEMENTS

Part of the work described in this paper was supported by the National Research Council PILP programs DHC-PILP 84-1 and 84-2. The author wishes to thank J.R. Digney of NAE and R.J.D.Poole of The de Havilland Aircraft of Canada, for co-operation during the course of this project and for making their experimental data available.

8.0 REFERENCES

[1] Capelier, C., Chevallier, J.P., and Bouniol, F., "Nouvelle méthode de correction des effets de parois en courant plan," La recherche aérospatiale, Jan.-Feb. 1978, pp.1-11.

[2] Ashill, P.R. and Weeks, D.J., "A Method for Determining Wall-Interference Corrections in Solid-Wall Wind Tunnels from Measurements of Static Pressure at the Walls," Wall Interference in Wind Tunnels, AGARD-CP-335, May 1982, pp.1.1-1.12.

[3] Hackett, J.E., Wilsden, D.J., and Lilley, D.E., "Estimation of Tunnel Blockage from Wall Pressure Signatures: A Review and Data Correlation," NASA CR-15, 224, March 1979.

[4] Kemp, W.B., "A Slotted Test Section Numerical Model for Interference Assessment," Journal of Aircraft, Vol.22, March 1985, pp.216-222.

[5] Rizk, M.H. and Murman, E.M., "Wind Tunnel Wall Interference Corrections for Aircraft Models in the Transonic Regime," Journal of Aircraft, Vol.21, Jan.1984, pp.54-61.

[6] Sawada, H., "Wind Tunnel Wall Interference in a Test Section with Ventilated Walls," 12th Congress of the International Council of the Aeronautical Sciences, Munich, Oct.1980.

[7] Mokry, M., "Subsonic Wall Interference Corrections for Finite-Length Test Sections Using Boundary Pressure Measurements," AGARD-CP-335, pp.10.1-10.15, May 1982.

[8] Rizk, M.H. and Smithmeyer, M.G., "Wind-Tunnel Interference Corrections for Three-Dimensional Flows," Journal of Aircraft, Vol.19, June 1982, pp.465-472.

[9] Mokry, M., Peake, D.J., and Bowker, A.J., "Wall Interference on Two-Dimensional Supercritical Airfoils, Using Wall Pressure Measurements to Determine the Porosity Factors for Tunnel Floor and Ceiling," Aeronautical Rept. LR-575, National Research Council Canada, Feb.1974.

[10] Nenni, J.P, Erickson, J.C., and Wittliff, C.E., "Measurement of Small Normal Velocity Components in Subsonic Flow by Use of a Static Pipe," AIAA Journal, Vol.20, Aug.1982, pp.1077-1083.

[11] Firmin, M.C.P. and Cook, P.H., "Disturbances from Ventilated Tunnel in Aerofoil Testing," AGARD-CP-348, Sept.1983, pp.8.1-8.15.

[12] Berndt, S.B., "Measuring the Flow Properties of Slotted Test-Section Walls," FFA 135, The Aeronautical Research Institute of Sweden, May 1982.

[13] Baldwin, B.S., Turner, J.B., and Knechtel, E.D., "Wall Interference in Wind Tunnels With Slotted and Porous Boundaries at Subsonic Speeds," NACA TN-3176, 1954.

[14] Mokry, M. and Ohman, L.H., "Application of the Fast Fourier Transform to Two-Dimensional Wind Tunnel Wall Interference," Journal of Aircraft, Vol.17, June 1980, pp.402-408.

[15] Starr, R.F., "Experimental Observations of Wall Interference at Transonic Speeds," AIAA Paper 78-164, Jan.1978.

[16] Garner, H.C., Rogers, E.W.E., Acum, W.E.A., and Maskell, E.C., "Subsonic Wind Tunnel Wall Corrections," AGARDograph 109, Oct.1966.

[17] Boersen S.J. and Elsenaar, A., "Half-Model Testing in the NLR High Speed Wind Tunnel HST : Its Technique and Application," AGARD-CP-348 Wind Tunnels and Testing Techniques, Sept.1983, pp.23.1-23.15.

[18] Stakgold, I., *Green's Functions and Boundary Value Problems*, John Wiley, 1979, pp.513-514.

[19] Mokry, M. and Galway, R.D., "Analysis of Wall Interference Effects on ONERA Calibration Models in the NAE 5-ft. x 5-ft. Wind Tunnel," Aeronautical Rept. LR-594, National Research Council Canada, March 1977.

[20] Digney, J.R., "Phase 1 Test of the Dehavilland 'WTDR' Half-Model in the 5-ft Wind Tunnel," LTR-HA-5 $\times$ 5/0143, National Aeronautical Establishment, National Research Council Canada, Sept.1983.

[21] Khalid, M., "Investigation of Half-Wing Augmentor Model WTHW in the 5 ft $\times$ 5 ft Test Facility," LTR-HA-5 $\times$ 5/0150, National Aeronautical Establishment, National Research Council Canada, Aug.1984.

[22] Pounds, G.A. and Walker, J., "Semispan Model Testing in a Variable Porosity Transonic Wind Tunnel," AIAA Paper No.80-0461, 1980.

[23] Hinson, B.L. and Burdges, K.P., "Acquisition and Application of Transonic Wing and Far-Field Test Data for Three-Dimensional Computational Method Evaluation," AFOSR-TR-80-0421, Lockheed-Georgia Co., March 1980.

[24] Hinson, B.L. and Burdges, K.P., "Evaluation of Three-Dimensional Transonic Codes Using New Correlation-Tailored Test Data," Journal of Aircraft, Vol.18, Oct.1981, pp.855-861.

[25] "Experimental Data Base for Computers Program Assessment", AGARD-AR138-Addendum, July 1984, pp.B6-1 – B6-22.

[26] Ballhaus, W.F., Bailey, F.R., and Frick, J., "Improved Computational Treatment of Transonic Flow About Swept Wings," NASA CP-2001, Nov.1976.

[27] Milne-Thomson, L.M., *Theoretical Hydrodynamics*, 2nd ed., Macmillan 1950, pp.411-412.

[28] Vallentine, H.R., *Applied Hydrodynamics*,

[29] Greenspan, D., *Discrete Numerical Methods in Physics and Engineering*, Academic Press, 1974, pp.12-22. 2nd ed., Butterworth 1967, pp.249-251.

[30] Kuo, C.C. and Morino, L., "Steady Subsonic Flow Around Finite-Thickness Wings," NASA CR-2616, Nov.1975.

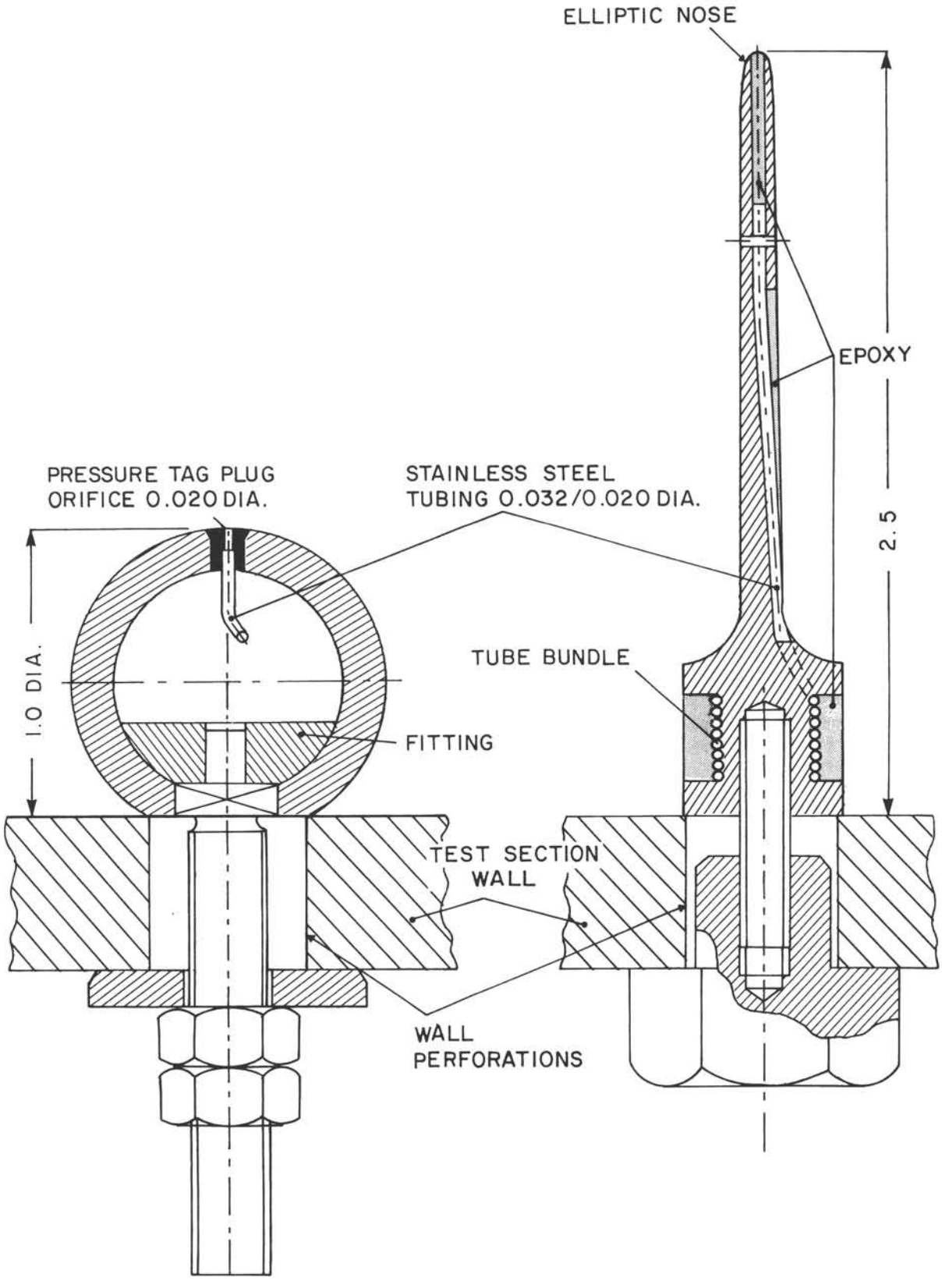

FIG. 1: CROSS-SECTIONS OF NAE STATIC PRESSURE DEVICES

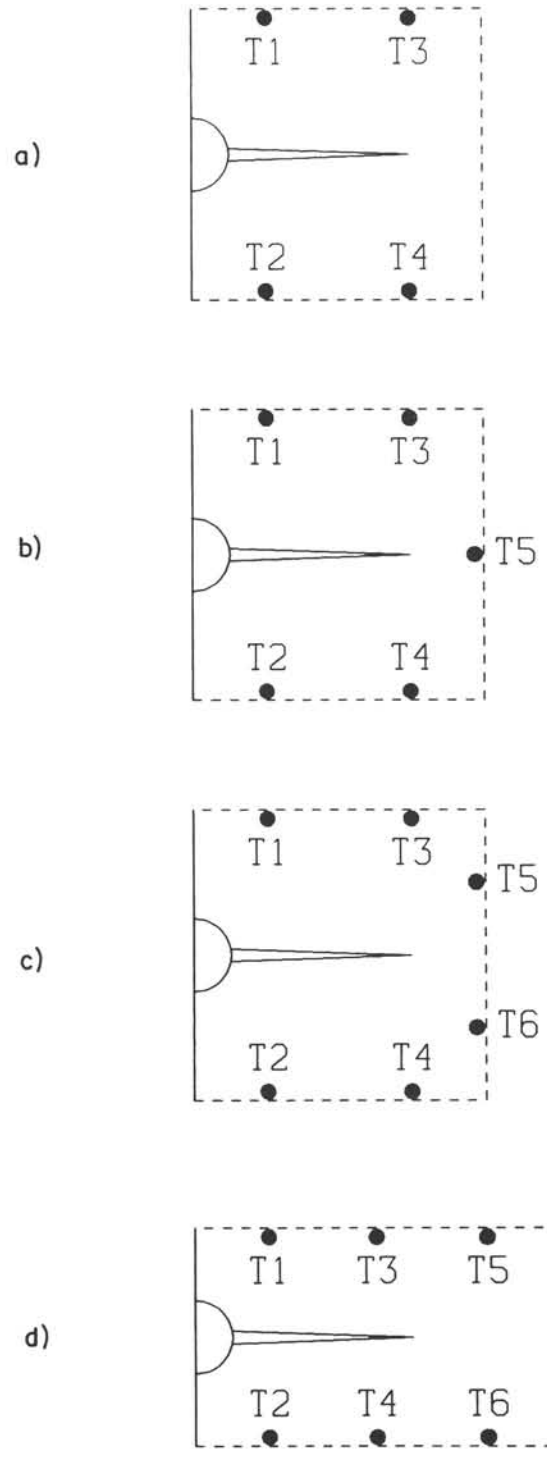

FIG. 2: LOCATION OF STATIC PRESSURE TUBES

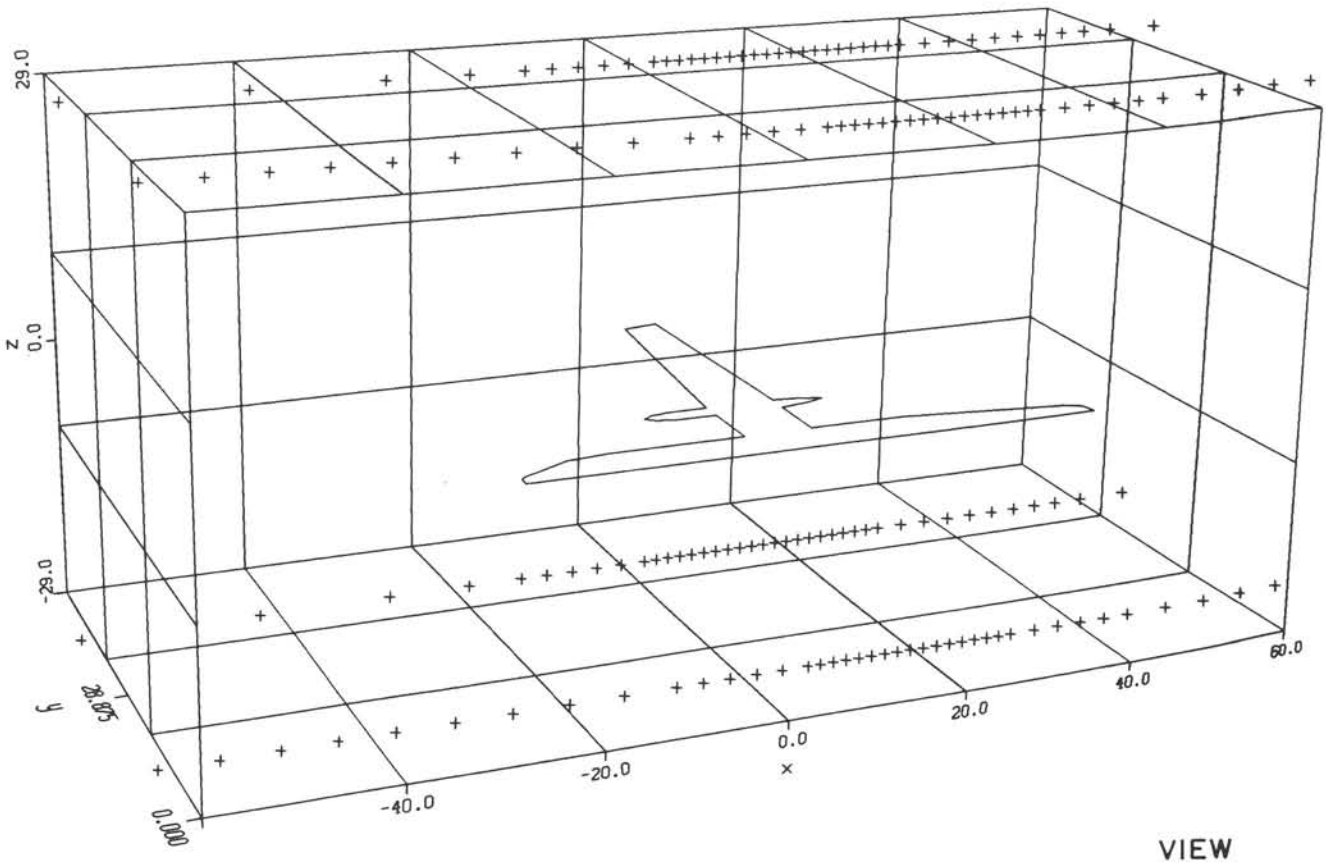

72 PANELS

VIEW
X = -120.00
Y = -240.00
Z = 96.00

FIG. 3a: TEST SECTION PANELLING, 3D VIEW (72 PANELS)

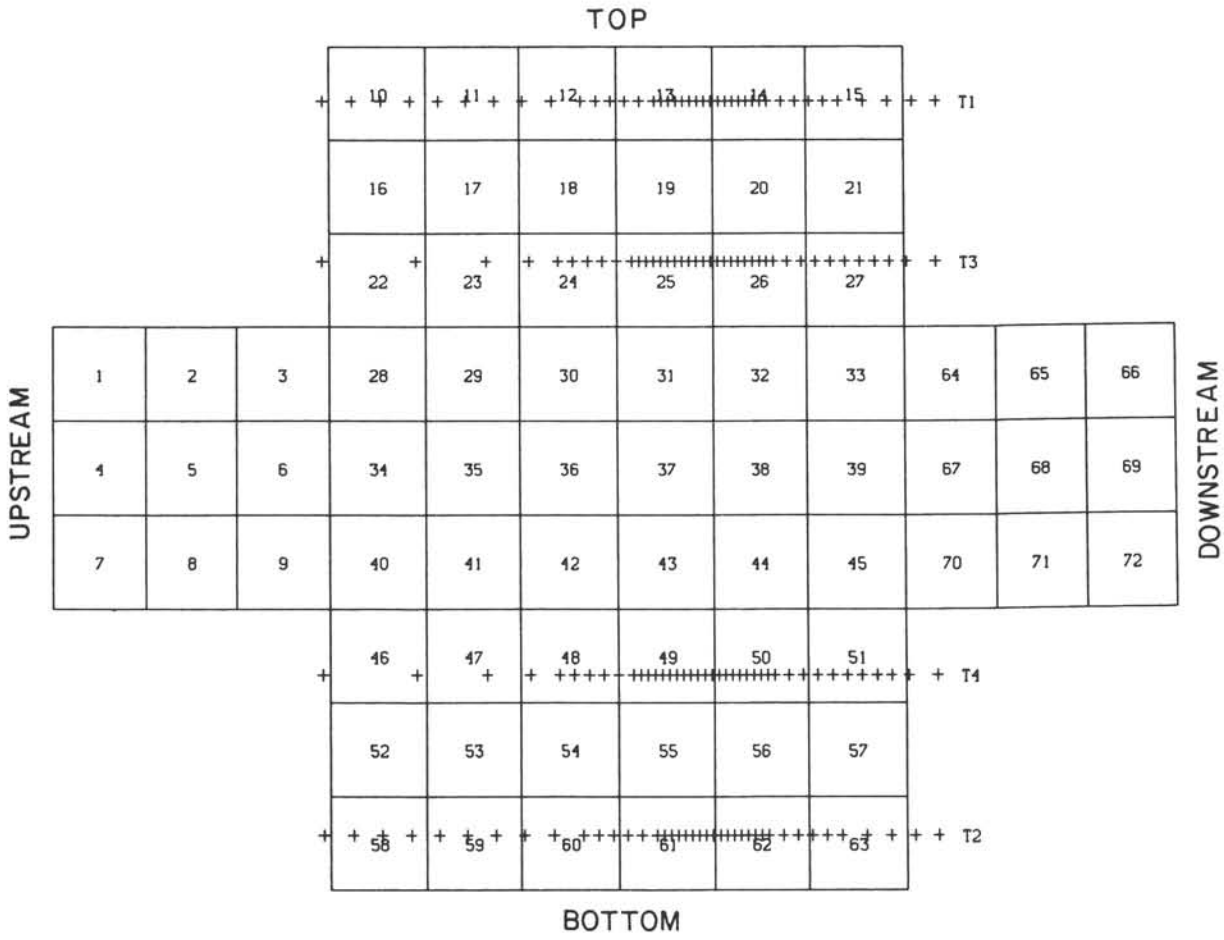

FIG. 3b: TEST SECTION PANELLING, UNFOLDED (72 PANELS)

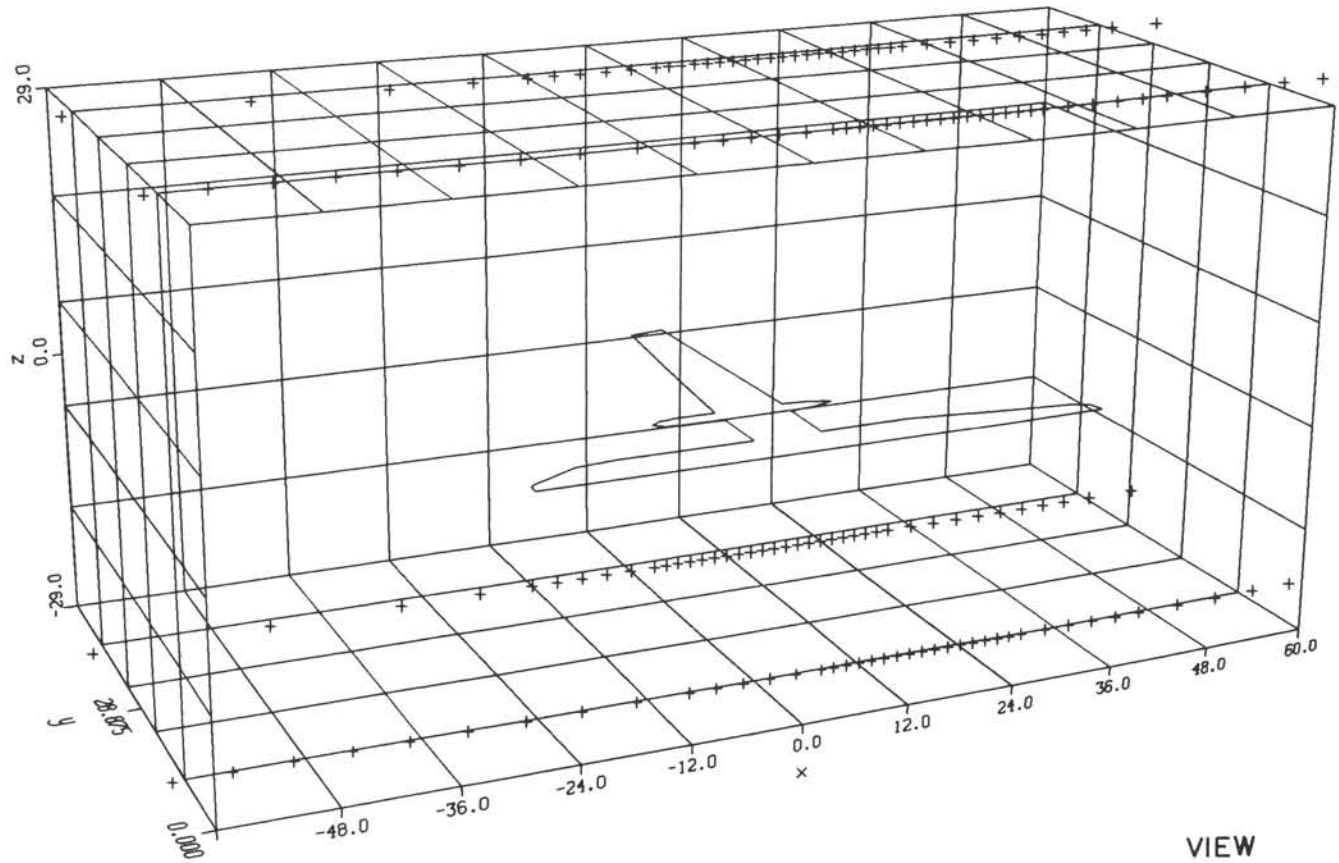

FIG. 4a: TEST SECTION PANELLING, 3D VIEW (200 PANELS)

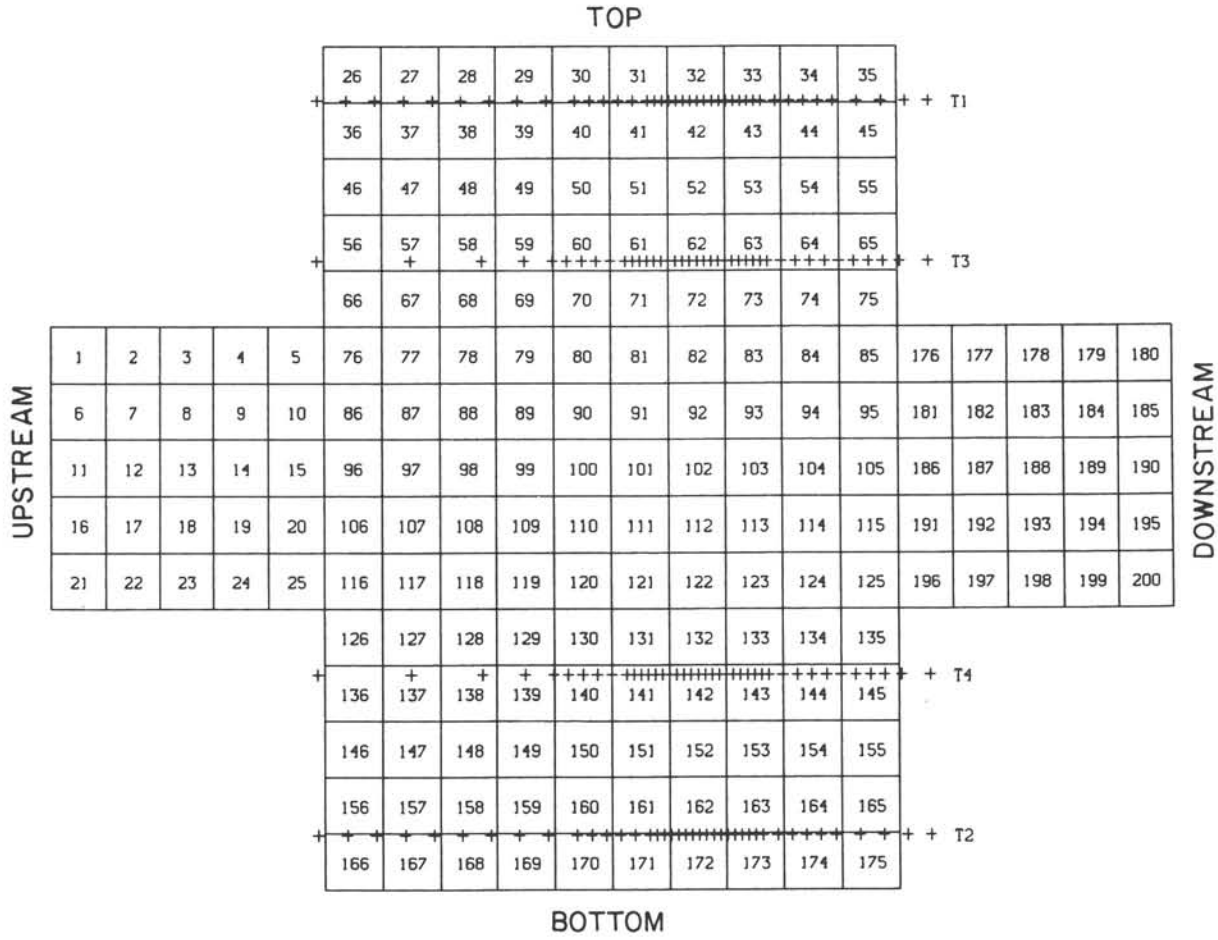

FIG. 4b: TEST SECTION PANELLING, UNFOLDED (200 PANELS)

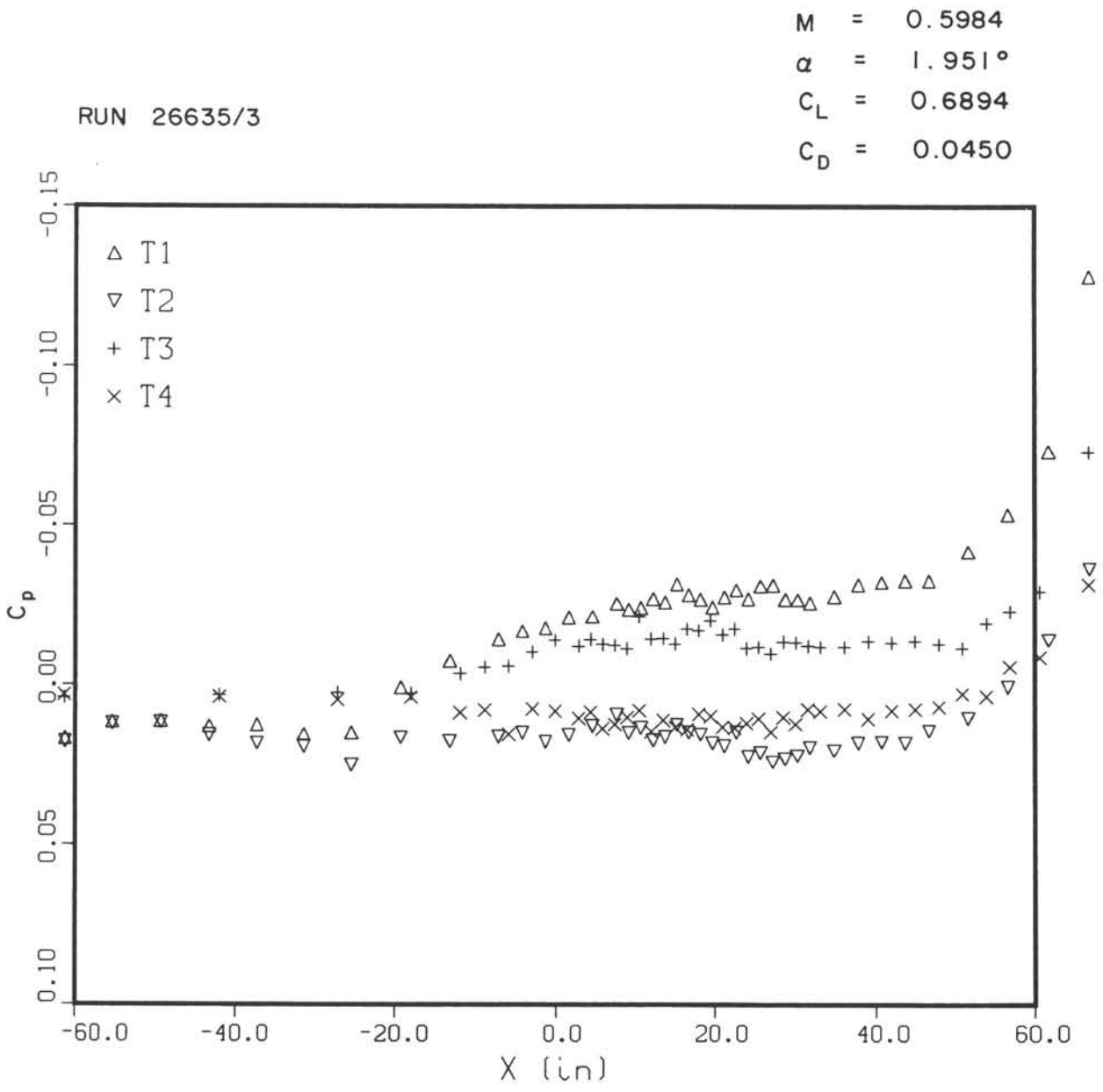

FIG. 5: TUBE PRESSURE DISTRIBUTIONS, M = 0.60, α = 1.95°

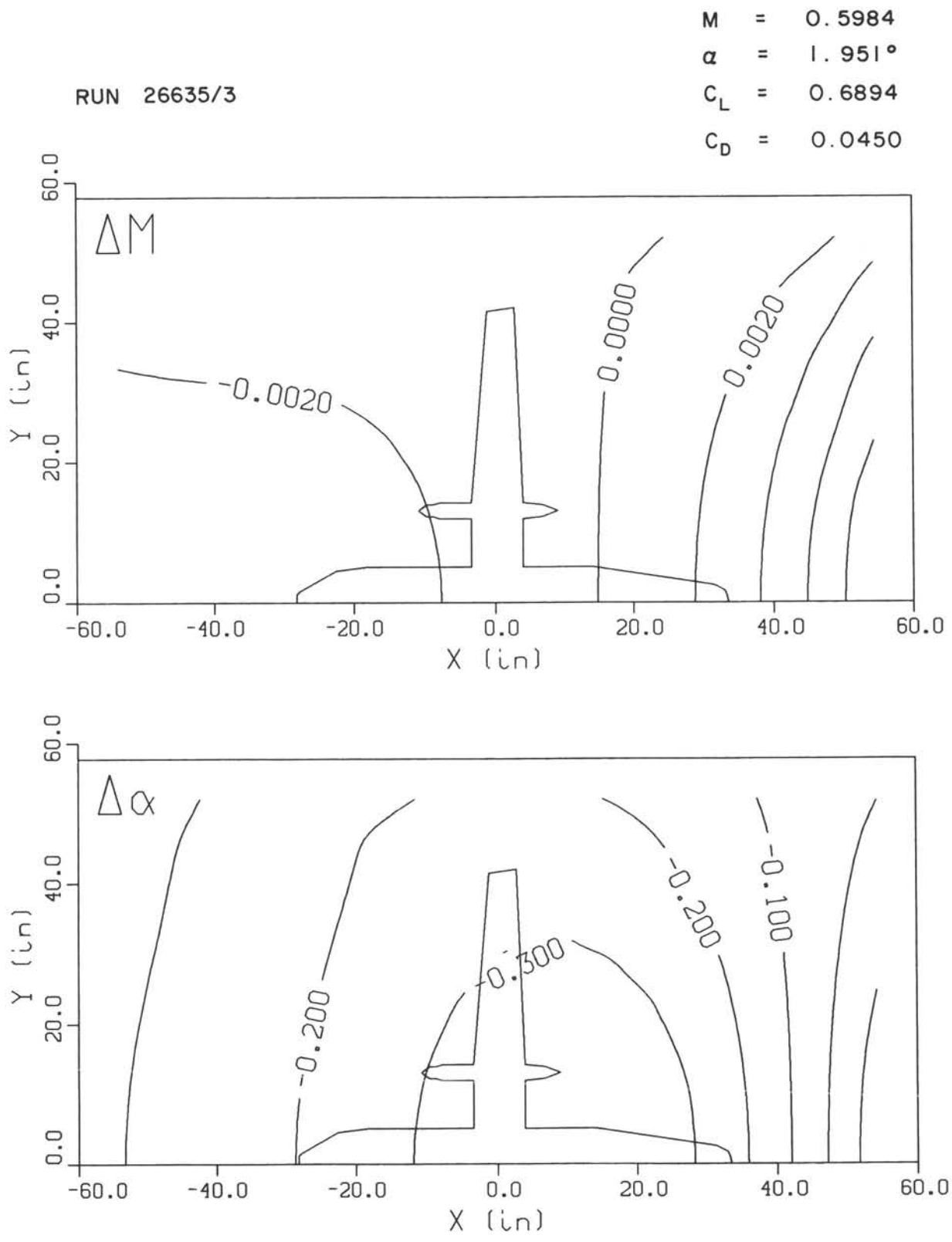

FIG. 6: MACH NUMBER AND ANGLE OF ATTACK CORRECTIONS, M = 0.60, α = 1.95° (72 PANELS)

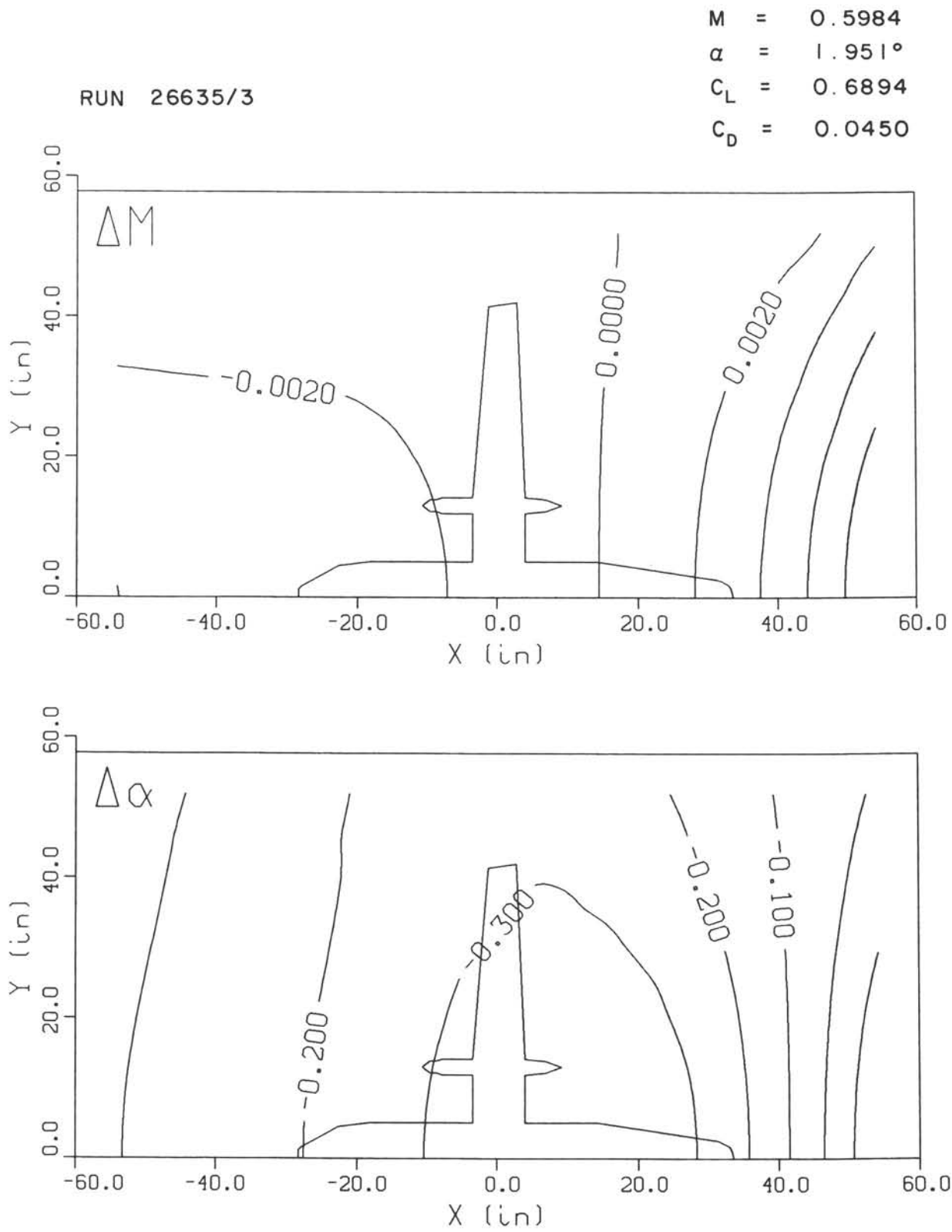

FIG. 7: MACH NUMBER AND ANGLE OF ATTACK CORRECTIONS, M = 0.60, α = 1.95° (200 PANELS)

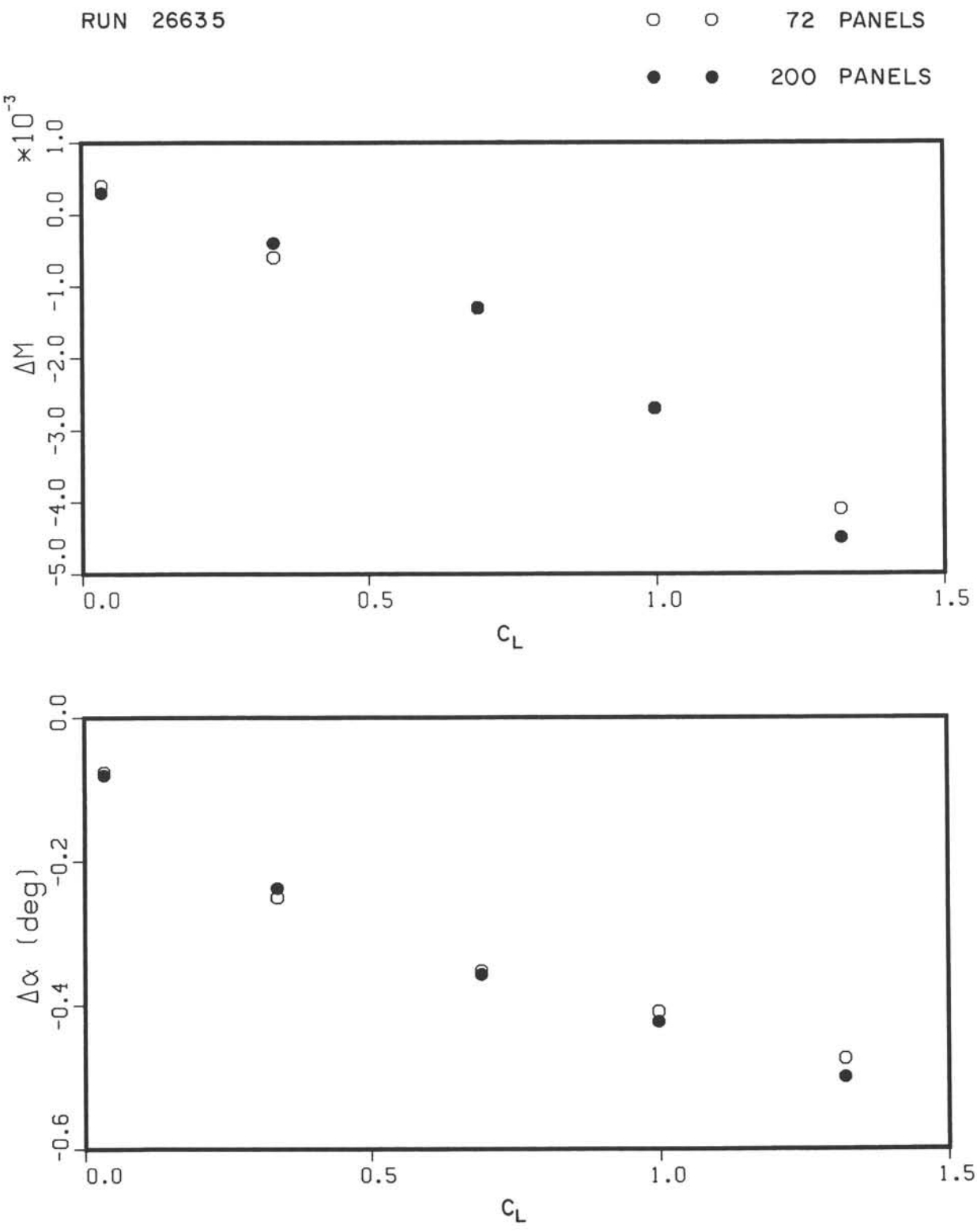

FIG. 8: MACH NUMBER AND ANGLE OF ATTACK CORRECTIONS AT THE CENTRE OF WING LOAD, M = 0.60

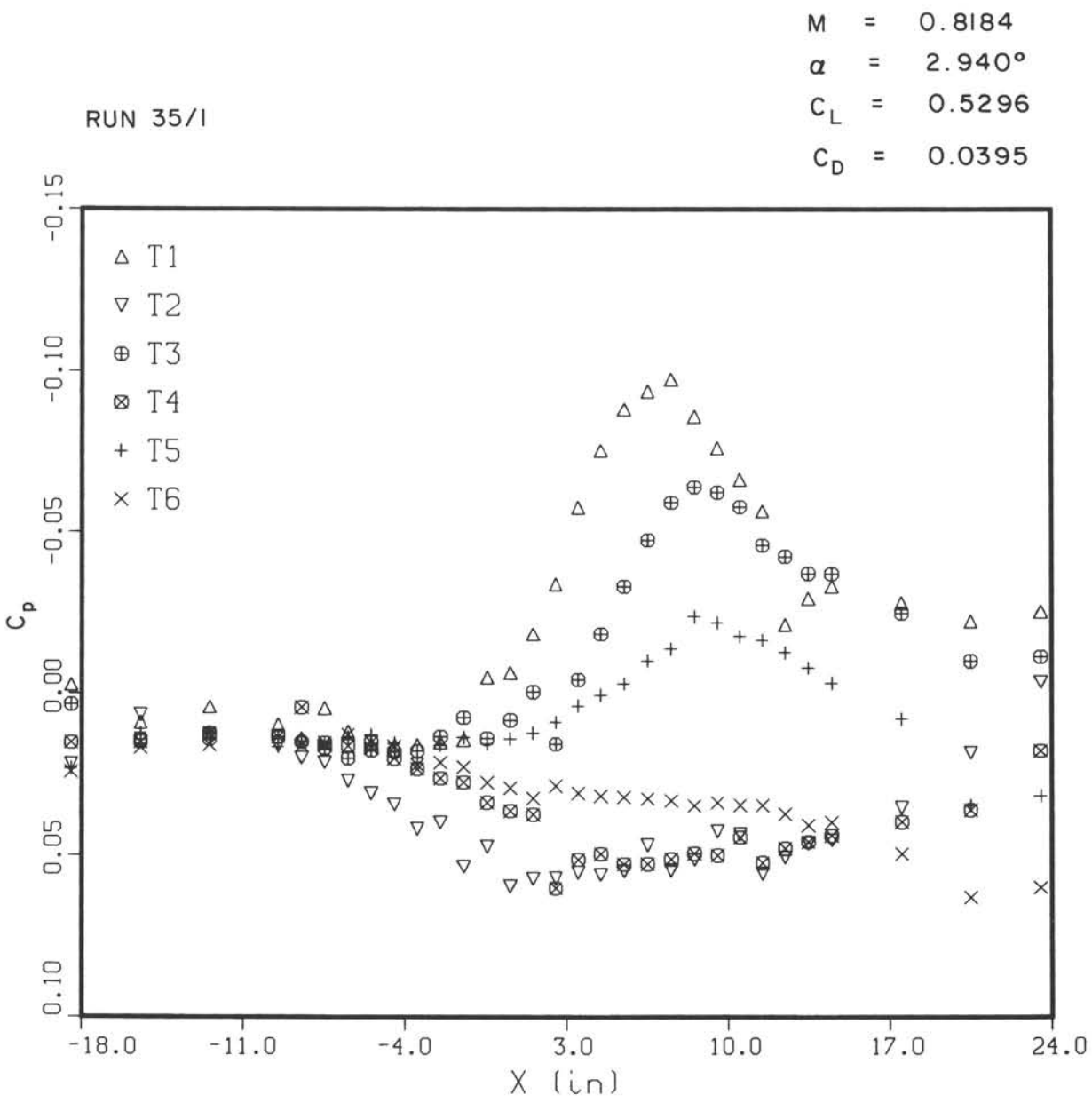

FIG. 9: RAIL PRESSURE DISTRIBUTIONS, WING "A", M = 0.82, α = 2.94°

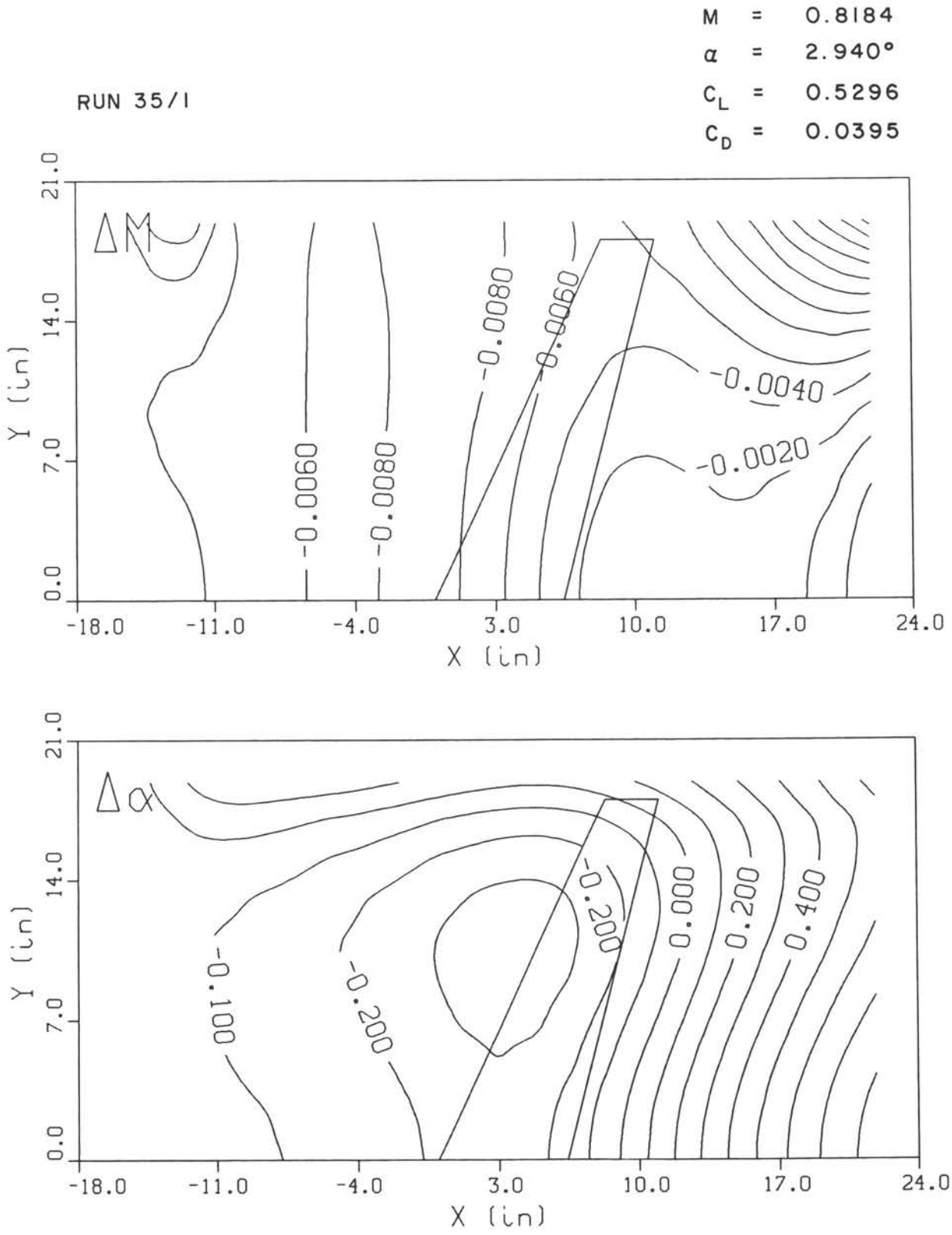

FIG. 10: MACH NUMBER AND ANGLE OF ATTACK CORRECTIONS, WING "A", M = 0.82, α = 2.94°

APPENDIX 1: FARFIELD REPRESENTATION OF THE MODEL

The calculation of boundary values of u from Eq.(2.6) requires, in addition to the measured pressure coefficients, also knowledge of the streamwise derivative of the free air disturbance velocity potential ϕ_F.

The disturbance velocity potential due to a wing of moderate to large aspect ratio, observed at a farfield point (X, Y, Z), can be represented by discrete singularities located at points (X_m, Y_m, Z_m) distributed along the quarter-chord line.

In accordance with the lifting line theory, the disturbance velocity potential associated with lift can be approximated by a discrete distribution of horseshoe vortices

$$\phi_F^L(X,Y,Z) = \frac{1}{4\pi}\sum_m \Gamma_m \frac{Z-Z_m}{(Y-Y_m)^2+(Z-Z_m)^2} \times \left(1+\frac{X-X_m}{\sqrt{(X-X_m)^2+\beta^2(Y-Y_m)^2+\beta^2(Z-Z_m)^2}}\right).$$

The individual strengths Γ_m are obtained from the spanwise wing load distribution. The total strength (circulation) satisfies

$$\Gamma = \sum_m \Gamma_m = \frac{1}{2} A C_L,$$

where C_L is the lift coefficient of the wing and A is the reference area on which it is based.

Similarly, the farfield associated with drag can be represented by a discrete distribution of sources

$$\phi_F^D(X,Y,Z) = -\frac{1}{4\pi}\sum_m \sigma_m \frac{1}{\sqrt{(X-X_m)^2+\beta^2(Y-Y_m)^2+\beta^2(Z-Z_m)^2}}.$$

The total source strength satisfies

$$\sigma = \sum_m \sigma_m = \frac{1}{2} A C_D,$$

and C_D is the (wake) drag coefficient of the wing.

Finally, the farfield associated with the volume effect of the wing can be represented by a discrete distribution of doublets

$$\phi_F^V(X,Y,Z) = \frac{1}{4\pi}\sum_m V_m \frac{X-X_m}{[(X-X_m)^2+\beta^2(Y-Y_m)^2+\beta^2(Z-Z_m)^2]^{3/2}},$$

where

$$V = \sum_m V_m$$

is the total volume of the wing. Alternative expressions for the disturbance velocity potential due to wings can be found in Ref.[8].

The fuselage or nacelle can be modelled by sources and sinks, for example as described in Ref.[3]. The simplest case is a Rankine body, generated by a source and a sink of equal strengths on a line parallel to the stream direction. Thus for a source located at $(-E,0,0)$ and a sink at $(E,0,0)$, the disturbance velocity potential is given by

$$\phi_F^B(X,Y,Z) = \frac{\mu}{4\pi}\left[\frac{-1}{\sqrt{(X+E)^2+\beta^2Y^2+\beta^2Z^2}} + \frac{1}{\sqrt{(X-E)^2+\beta^2Y^2+\beta^2Z^2}}\right].$$

The half-axes A and B can be determined by evaluating the stagnation point distance and the maximum deflection of the dividing streamline respectively [27],[28]. The half-axes A and B and the "eccentricity" E are found to be interrelated by

$$ab^2(\varepsilon+b) = (a-\varepsilon)^4$$

where

$$\varepsilon = E^2, \quad a = A^2, \quad \text{and} \quad b = \beta^2B^2.$$

Specifying the half-axes to approximate the shape of the body, ε can be evaluated in a few iterations by the generalized Newton's method [29], using

$$\varepsilon^{(0)} = \left(A - \frac{\beta B}{2}\right)^2$$

as the initial guess. The singularity strength μ follows from

$$\mu = \pi\frac{(A^2-E^2)^2}{AE}.$$

The farfield potential, combining the above effects, is then given by the sum

$$\phi_F = \phi_F^L + \phi_F^D + \phi_F^V + \phi_F^B.$$

APPENDIX 2: VELOCITY INDUCED BY A RECTANGULAR PANEL

The analysis is greatly simplified by introducing local coordinates ξ,η,ς, with ς along the (outward) normal to the panel. The streamwise velocity component at the point ξ_o,η_o,ς_o, induced by a rectangular panel $\xi_1<\xi<\xi_2$, $\eta_1<\eta<\eta_2$, $\varsigma=0$ of unit doublet density is

$$\begin{aligned}\tilde{u}(\xi_o,\eta_o,\varsigma_o) &= \int_{\eta_1}^{\eta_2}\int_{\xi_1}^{\xi_2}\frac{\partial}{\partial\varsigma}\frac{1}{4\pi\sqrt{(\xi_o-\xi)^2+(\eta_o-\eta)^2+(\varsigma_o-\varsigma)^2}}\Big|_{\varsigma=0}d\xi d\eta \\ &= \frac{\varsigma_o}{4\pi}\int_{\eta_1}^{\eta_2}\int_{\xi_1}^{\xi_2}\frac{1}{[(\xi_o-\xi)^2+(\eta_o-\eta)^2+\varsigma_o^2]^{3/2}}d\xi d\eta \\ &= -\frac{\varsigma_o}{4\pi}\int_{\eta_1}^{\eta_2}\frac{1}{(\eta_o-\eta)^2+\varsigma_o^2}\left[\frac{\xi_o-\xi}{\sqrt{(\xi_o-\xi)^2+(\eta_o-\eta)^2+\varsigma_o^2}}\right]_{\xi=\xi_1}^{\xi=\xi_2}d\eta,\end{aligned}$$

revealing familiar features of a vortex-type singularity. The remaining integration is performed with the help of the indefinite integral

$$\int \frac{dY}{(Y^2+A^2)\sqrt{Y^2+A^2+B^2}} = \frac{1}{AB}\arctan\left[\frac{B}{A}\frac{Y}{\sqrt{Y^2+A^2+B^2}}\right].$$

The result is

$$\begin{aligned}\tilde{u}(\xi_o,\eta_o,\varsigma_o) = \frac{1}{4\pi}\Bigg\{ &\arctan\left[\frac{\xi_o-\xi_1}{\varsigma_o}\frac{\eta_o-\eta_1}{\sqrt{(\xi_o-\xi_1)^2+(\eta_o-\eta_1)^2+\varsigma_o^2}}\right] \\ &-\arctan\left[\frac{\xi_o-\xi_1}{\varsigma_o}\frac{\eta_o-\eta_2}{\sqrt{(\xi_o-\xi_1)^2+(\eta_o-\eta_2)^2+\varsigma_o^2}}\right] \\ &-\arctan\left[\frac{\xi_o-\xi_2}{\varsigma_o}\frac{\eta_o-\eta_1}{\sqrt{(\xi_o-\xi_2)^2+(\eta_o-\eta_1)^2+\varsigma_o^2}}\right] \\ &+\arctan\left[\frac{\xi_o-\xi_2}{\varsigma_o}\frac{\eta_o-\eta_2}{\sqrt{(\xi_o-\xi_2)^2+(\eta_o-\eta_2)^2+\varsigma_o^2}}\right]\Bigg\}.\end{aligned}$$

Considering the principal value of the arctangent function, it is easily verified that

$$\lim_{\varsigma_o\to 0\pm}\tilde{u} = \begin{cases}\pm\frac{1}{2}, & \text{on the panel;}\\ 0, & \text{outside the panel,}\end{cases}$$

in accordance with Eq.(3.6).

In Ref.[30], a similar formula is given for the trapezoidal doublet panel, which can be used for more general test section geometries.